JACS
JOURNAL OF THE AMERICAN CHEMICAL SOCIETY

Article

pubs.acs.org/JACS

Manganese Electrocatalysts with Bulky Bipyridine Ligands: Utilizing Lewis Acids To Promote Carbon Dioxide Reduction at Low Overpotentials

Matthew D. Sampson and Clifford P. Kubiak*

Department of Chemistry and Biochemistry, University of California, San Diego, 9500 Gilman Drive, Mail Code 0358, La Jolla, California 92093-0358, United States

Supporting Information

ABSTRACT: Earth-abundant manganese bipyridine (bpy) complexes are well-established molecular electrocatalysts for proton-coupled carbon dioxide (CO_2) reduction to carbon monoxide (CO). Recently, a bulky bipyridine ligand, 6,6′-dimesityl-2,2′-bipyridine (mesbpy), was utilized to significantly lower the potential necessary to access the doubly reduced states of these manganese catalysts by eliminating their ability to dimerize after one-electron reduction. Although this Mn mesbpy catalyst binds CO_2 at very low potentials, reduction of a resulting Mn(I)−COOH complex at significantly more negative potentials is required to achieve fast catalytic rates. Without reduction of Mn(I)−COOH, catalysis occurs slowly via a alternate catalytic pathway−protonation of Mn(I)−COOH to form a cationic tetracarbonyl complex. We report the use of Lewis acids, specifically Mg^{2+} cations, to significantly increase the rate of catalysis (by over 10-fold) at these low overpotentials (i.e., the same potential as CO_2 binding). Reduction of CO_2 occurs at one of the lowest overpotentials ever reported for molecular electrocatalysts (η = 0.3−0.45 V). With Mg^{2+}, catalysis proceeds via a reductive disproportionation reaction of $2CO_2 + 2e^- \rightarrow CO + CO_3^{2-}$. Insights into the catalytic mechanism were gained by using variable concentration cyclic voltammetry, infrared spectroelectrochemistry, and bulk electrolysis studies. The catalytic Tafel behavior (log turnover frequency vs overpotential relationship) of [Mn(mesbpy)(CO)$_3$(MeCN)](OTf) with added Mg^{2+} is compared with those of other commonly studied CO_2 reduction catalysts.

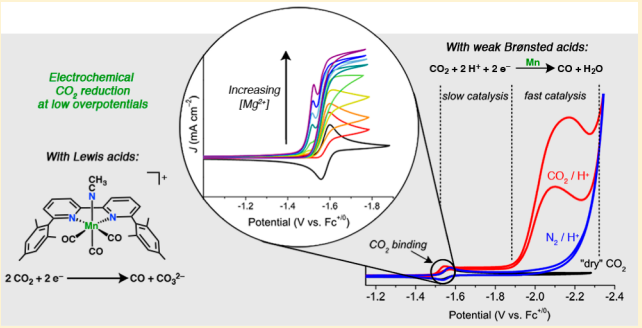

INTRODUCTION

Depletion of fossil fuel resources along with unsustainable, anthropogenic emissions of carbon dioxide (CO_2) requires the development of renewable, carbon-neutral fuels. Extensive research and development has been put forth to employ technologies for solar and wind power. However, these energy sources suffer from intermittent availability, and therefore, there is a demand to develop efficient and recoverable methods for storing electrical energy in chemical bonds. In this regard, the electrocatalytic CO_2 reduction is one of the most attractive approaches. Here, a renewable energy source, such as sunlight or wind, can be used to drive an electrochemical reaction, converting CO_2 into energy-dense carbon compounds, which can be utilized as fuels and chemical feedstocks.[1−3]

Reductions of CO_2 are typically coupled with protons to overcome high thermodynamic thresholds, which originate from transferring a single electron to CO_2 (to form $CO_2^{\bullet-}$). However, these proton-coupled, multielectron conversions are plagued with slow kinetics, and therefore, efficient catalysts are required to decrease the overpotentials needed to drive the reactions. Molecular catalysts are highly attractive for electrocatalytic processes for the following reasons: (1) these catalysts are both highly active and selective for the specific catalytic process, (2) reaction intermediates are comparatively easy to spectroscopically characterize, allowing for elucidation of mechanistic details of the catalytic reactions, and (3) variation of the catalyst structure to suit the appropriate catalytic process can be achieved in a straightforward manner through synthetic means. Recent work has focused on heterogenizing molecular catalysts to increase lifetimes of the catalytic systems and facilitate separation of the catalysts with final products.[4−9]

Re[10−23] and Mn[24−28] bipyridine (bpy) complexes have garnered significant interest in recent years as CO_2 reduction catalysts. These catalysts are among the most active and selective molecular electrocatalysts for proton-coupled CO_2 reduction to carbon monoxide (CO). However, these catalysts suffer from high overpotentials, which originate from the potentials required to access their active, doubly-reduced states.[18,27,29] Mn bpy catalysts are desirable, in comparison with their Re analogs, due to the earth-abundance (and thus low cost) of Mn and the ability for these catalysts to operate at lower overpotentials (i.e., less energy is needed to drive their catalytic reactions). Mn bpy complexes have also been used

Received: November 22, 2015
Published: January 8, 2016

DOI: 10.1021/jacs.5b12215
J. Am. Chem. Soc. 2016, 138, 1386−1393

recently as catalysts in photochemical reduction of CO_2 to formate utilizing TEOA as an H atom donor.[30,31]

Previously, our group reported electrocatalytic CO_2 reduction by a pair of Mn complexes with bulky bpy ligands, $Mn(mesbpy)(CO)_3Br$ (**1**; mesbpy =6,6′-dimesityl-2,2′-bipyridine) and $[Mn(mesbpy)(CO)_3(MeCN)](OTf)$ (**2**, MeCN = acetonitrile; OTf = trifluoromethanesulfonate).[28] The structures of complexes **1** and **2** are shown in Figure 1. In contrast to

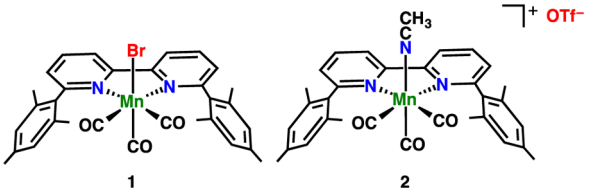

Figure 1. Schematic of the molecular structures of **1** and **2**.

typical $Mn(bpy\text{-}R)(CO)_3X$ complexes, **1** and **2** do not dimerize after one-electron reduction (eq 1), which significantly lowers the potential necessary to access their doubly-reduced, anionic states (by ∼300 mV).[32] Moreover, **1** and **2** undergo a single, two-electron reduction (eq 3) rather than two separate one-electron reductions (eqs 1 and 2) to access their doubly-reduced states:

$$Mn^{I}(bpy)(CO)_3Br + e^- \rightarrow 1/2[Mn^{0}(bpy)(CO)_3]_2 + Br^- \quad (1)$$

$$1/2[Mn^{0}(bpy)(CO)_3]_2 + e^- \rightarrow [Mn(bpy)(CO)_3]^- \quad (2)$$

$$Mn^{I}(mesbpy)(CO)_3Br + 2e^- \rightarrow [Mn(mesbpy)(CO)_3]^- + Br^- \quad (3)$$

The doubly-reduced states for complexes **1** and **2** bind CO_2 in the presence of weak Brønsted acids (Figure 2) to form a Mn(I)−COOH complex.[28] Upon forming this Mn(I)−COOH complex, catalysis does not proceed with significant rates until a

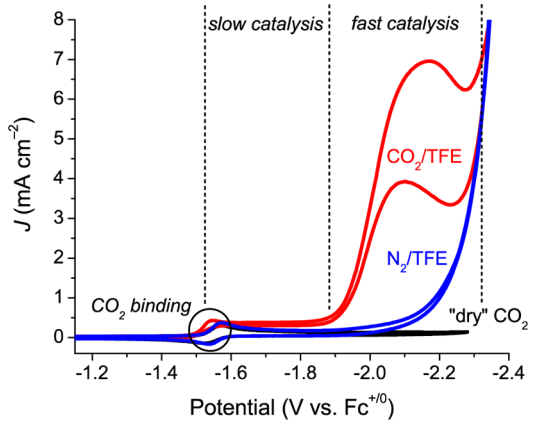

Figure 2. Cyclic voltammograms of $[Mn(mesbpy)(CO)_3(MeCN)](OTf)$ (**2**) under CO_2 without added weak acid (black) and under CO_2 with added 1.3 M TFE (red). Two regions are depicted in the figure. Under N_2 with added TFE, no current increase is observed until a much more negative potential (blue). Conditions: 0.1 M $TBAPF_6$/MeCN; ν = 0.1 V/s; working electrode = glassy carbon; counter electrode = Pt; reference electrode = Ag/AgCl; ferrocene (Fc) added as an internal reference.

∼400 mV more negative potential (Figure 2). Our previous infrared spectroelectrochemistry (IR-SEC) experiments suggest that this unusual "over-reduction" is necessary to reduce the Mn(I)−COOH complex, which is needed to drive catalysis. At these more negative potentials, **1** and **2** are highly active for CO_2 reduction, reaching rates of ∼5000 s^{-1} with trifluoroethanol (TFE) as a proton source.[28]

At potentials between CO_2 binding and "fast catalysis" (see the large catalytic wave in Figure 2), it is likely that "slow catalysis" occurs via an alternate mechanism. After forming a Mn(I)−COOH complex from CO_2 binding by $[Mn(mesbpy)(CO)_3]^-$ followed by protonation, this species can be further protonated to cleave one C−O bond and form a cationic $[Mn^{I}(mesbpy)(CO)_4]^+$ complex. This tetracarbonyl complex can be easily reduced at these potentials to release CO and regenerate $[Mn(mesbpy)(CO)_3]^-$. Previous computational studies have shown that Mn bpy complexes can operate via these two pathways.[29] Recently, we have also used the mesbpy ligand to isolate a highly active homogeneous Ru electrocatalyst, which typically polymerizes on electrode surfaces without bulky substituents on bpy.[33] Around the same time, Kuramochi et al. reported the photocatalytic CO_2 reduction activity of the same Ru complex.[34]

Since reporting the electrocatalytic CO_2 reduction activity of **1** and **2** in 2014, we have explored a few strategies to increase the rate of catalysis in this "slow catalysis" regime (near −1.6 V vs $Fc^{+/0}$, see Figure 2). One strategy was to utilize stronger Brønsted acids than H_2O, methanol, TFE, or phenol to promote faster C−O bond cleavage in the Mn(I)−COOH complex. Most acids stronger than phenol resulted in H^+ reduction catalysis rather than CO_2 reduction catalysis. Specifically, with a strong acid, such as trifluoroacetic acid (TFA), complex **2** is highly active for H^+ reduction at −1.6 V versus $Fc^{+/0}$, reaching rates of 5500 s^{-1}.[35]

In the early 1990s, Savéant and co-workers utilized Mg^{2+} cations as well as other Lewis acids to increase the rate of CO_2 reduction and greatly improve the stability of catalysis for Fe tetraphenylporphyrins (FeTPP).[36] These Lewis acids facilitate the breaking of one C−O bond of a bound CO_2 ligand to produce CO and both increase the stability and activity of catalysis. Herein, we report a similar technique, the use of Lewis acids in place of Brønsted acids, to increase the rate of catalysis in the "slow catalysis" regime for catalysts **1** and **2**. First, we demonstrate that slow catalysis occurs at −1.6 V versus $Fc^{+/0}$ with added TFE as a H^+ source. We further employ Mg^{2+} to alter the mechanism for CO_2 reduction by **1** and **2** and increase the rate of catalysis at these low overpotentials. Specifically, use of Mg^{2+} increases the maximum catalytic turnover frequency (TOF) by greater than 10-fold. We utilize IR-SEC under CO_2 to gain insight into the mechanism for catalysis with Mg^{2+}. Since this catalysis generates insoluble $MgCO_3$ during the reaction course, we employed a sacrificial Mg anode during bulk electrolysis experiments to stabilize catalysis over several hours. Finally, the Tafel behavior (log TOF vs overpotential relationship) of catalyst **2** is compared with those of other commonly studied CO_2 reduction catalysts.

RESULTS AND DISCUSSION

Synthesis and Characterization. Syntheses of mesbpy and complexes **1** and **2** were performed as previously reported.[28,37] Spectroscopic characterization by NMR and Fourier transform infrared (FTIR) were consistent with previous reports of complexes **1** and **2**.[28] The electrochemical

DOI: 10.1021/jacs.5b12215
J. Am. Chem. Soc. 2016, 138, 1386−1393

behaviors of complexes **1** and **2** have been described previously.[28] Notably, under inert atmosphere, complexes **1** and **2** undergo a single, two-electron reduction near −1.6 V versus $Fc^{+/0}$. This overall two-electron reduction generates the anionic complex $[Mn(mesbpy)(CO)_3]^-$. This doubly-reduced, anionic complex binds CO_2 in the presence of H^+ to form a Mn(I)−COOH complex; however, further reduction of this hydroxycarbonyl complex (at approximately −2.0 V vs $Fc^{+/0}$) is required to achieve fast catalytic rates to produce CO.

Controlled Potential Electrolysis (CPE) at Low Overpotential. To confirm that "slow catalysis" occurs at the potential of CO_2 binding (i.e., −1.6 V vs $Fc^{+/0}$), CPE was performed on complex **2** with 1.3 M TFE using a glassy carbon working electrode with large surface area (~80 cm^2). Indeed, under CO_2, slightly higher current densities were achieved with TFE than with "dry" CO_2 (Figure 3). Additionally, formation of

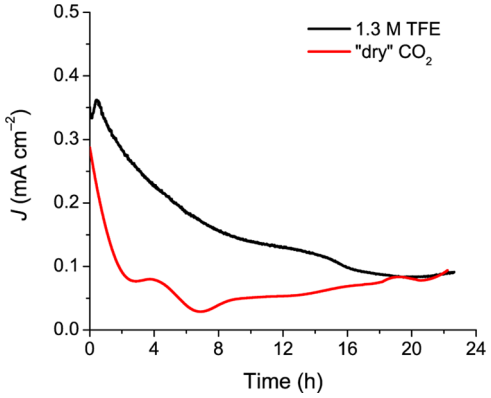

Figure 3. CPE current density over time for 0.5 mM $[Mn(mesbpy)(CO)_3(MeCN)](OTf)$ (**2**) under CO_2 with added 1.3 M TFE (black) and without added TFE (red). CPE is run at −1.6 V versus $Fc^{+/0}$, showing that slow catalysis does occur at this potential. Conditions: 0.1 M $TBAPF_6$/MeCN; working electrode = glassy carbon; counter electrode = Pt; reference electrode = Ag/AgCl.

CO in the headspace of the CPE cell was confirmed by gas chromatography (GC). Complex **2** operated with 96 ± 3% Faradaic efficiency for CO production from CO_2 (Figure S1). The turnover number (TON) of CO reached ~30 after 24 h of electrolysis (Figure S2), further confirming the slow rate of catalysis. In previous CPE experiments, **2** sustained over 10-fold higher current densities at −2.2 V versus $Fc^{+/0}$ over a similar time range with only 0.3 M TFE.[28] Minimal H_2 formation was observed over 24 h of electrolysis (TON of H_2 = ~0.06). CPE experiments at −1.6 V versus $Fc^{+/0}$ with "dry" CO_2 resulted in little CO formation (TON for CO = 0.5 after 24 h).

Cyclic Voltammograms (CVs) with Added Mg^{2+}. To investigate the ability of Lewis acids to increase rates of catalysis at the potential of CO_2 binding (i.e., −1.6 V vs $Fc^{+/0}$), CVs were recorded in the presence of $Mg(OTf)_2$. Electrocatalytic properties were studied in a custom-made, single-compartment, airtight cell with a glassy carbon working electrode, Pt wire counter electrode, and a Ag/AgCl leakless reference electrode (see Experimental Section for more details). As previously described, CVs of complex **2** do not change under CO_2 atmosphere in dry MeCN. Upon addition of Mg^{2+}, a current increase is observed near −1.6 V versus $Fc^{+/0}$ in CVs of **2** under CO_2 (Figure 4). This current increase corresponds to the electrocatalytic reduction of CO_2, as verified by CPE (vide infra). Under either inert atmosphere or CO_2, CVs of Mg^{2+}

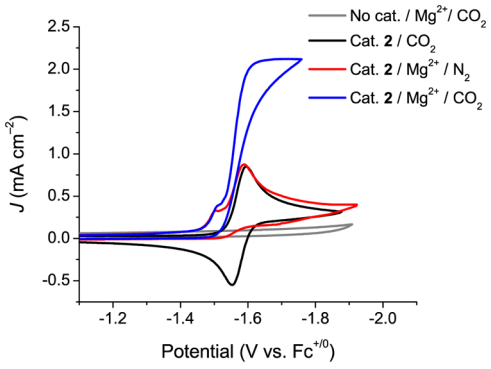

Figure 4. CVs of 1 mM $[Mn(mesbpy)(CO)_3(MeCN)](OTf)$ (**2**) under CO_2 without Mg^{2+} (black), under N_2 with 20 mM Mg^{2+} (red), and under CO_2 with 20 mM Mg^{2+} (blue). For reference, a CV without complex **2**, only with 20 mM Mg^{2+} under CO_2, is shown in gray. Catalytic current is only observed with all of the following: complex **2**, Mg^{2+}, and CO_2. Conditions: 0.1 M $TBAPF_6$/MeCN; ν = 0.1 V/s; working electrode = glassy carbon; counter electrode = Pt; reference electrode = Ag/AgCl; ferrocene (Fc) added as an internal reference.

without added Mn catalyst show no reductive reactivity in the window we are probing. Additionally, under N_2 atmosphere, no current increase is observed in CVs of **2** with added Mg^{2+} (Figure 4). Higher concentrations of Mg^{2+} in CVs resulted in increased current densities, up to a peak current density of approximately 2.7 mA cm^{-2} (Figure 5). Under N_2 atmosphere,

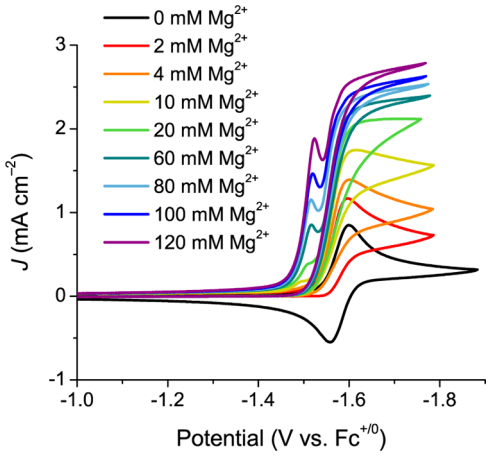

Figure 5. CVs of 1 mM $[Mn(mesbpy)(CO)_3(MeCN)](OTf)$ (**2**) under CO_2 with varying concentrations of Mg^{2+}, showing electrocatalytic reduction of CO_2. Conditions: 0.1 M $TBAPF_6$/MeCN; ν = 0.1 V/s; working electrode = glassy carbon; counter electrode = Pt; reference electrode = Ag/AgCl; ferrocene (Fc) added as an internal reference.

two interesting features are apparent in CVs of **2** with added Mg^{2+}: (1) a prewave exists prior to the two-electron reduction of **2**, which increases as $[Mg^{2+}]$ increases; (2) loss of reversibility of the two-electron reduction is observed (Figures 4, 5, and S3). These features are consistent with interaction between the singly- or doubly-reduced Mn complex and Mg^{2+} (vide infra).

The normalized peak catalytic current (i_{cat}/i_p) is related to the TOF of the catalytic reaction, as described in more detail in the Supporting Information. Using this relationship, we can estimate TOF values for catalyst **2** with added Mg^{2+}. Addition of 120 mM Mg^{2+} to a 1 mM solution of **2** under CO_2 resulted

DOI: 10.1021/jacs.5b12215
J. Am. Chem. Soc. 2016, 138, 1386−1393

in a peak i_{cat}/i_p = 3.5 and TOF = 20 s^{-1}. By using peak i_{cat}/i_p values as a metric for TOF, at peak activity, catalyst **2** operates with greater than 200-fold less activity at approximately −1.6 V versus $Fc^{+/0}$ with added Mg^{2+} than in the "fast catalysis" regime with added TFE (−2.1 V vs $Fc^{+/0}$, see Figure 2). However, catalyst **2** does operate with approximately 10-fold greater activity in the "slow catalysis" regime with added Mg^{2+} than with added TFE (with TFE at −1.6 V vs $Fc^{+/0}$, $i_{cat}/i_p \approx 1$, TOF ≈ 2). To gain further details about the catalytic mechanism, variable concentration CV studies were performed to obtain the rate of the catalytic reaction in [**2**], [CO_2], and [Mg^{2+}]. Plotting i_{cat} versus [**2**] shows a linear relationship, indicating that the catalytic reaction is first order in [**2**] (Figure S4). The electrocatalytic reaction is second order in [CO_2], as evidenced by plotting i_{cat} versus [CO_2] (Figure S5, see Supporting Information for relationship between i_{cat} and [substrate]). A plot of i_{cat} versus [Mg^{2+}] shows a first-order dependence on [Mg^{2+}] at low [Mg^{2+}] (Figure S6). At higher [Mg^{2+}], i_{cat} reaches a limiting value independent of [Mg^{2+}], which is typical of saturation kinetics expected for catalytic reactions.[38] The catalytic current plateaus in catalytic CVs with added Mg^{2+} are also scan rate independent (Figure S7), indicating that the catalytic reaction is at steady state. In summary, at high concentrations of [Mg^{2+}], the catalytic reaction is first order in **2**, second order in CO_2, and independent of Mg^{2+}.

Although rates of electrocatalysis with Mg^{2+} are not up to par with rates typically observed for Mn bpy catalysts at further negative potentials, any significant rate for catalysis at −1.6 V versus $Fc^{+/0}$ is noteworthy. Costentin et al. have calculated the standard reduction potential for the reduction of CO_2 to CO and HCO_3^{2-} where one CO_2 molecule serves as the weak acid: $2CO_2 + H_2O + 2e^- \rightarrow CO + HCO_3^- + OH^-$.[39] The mechanism for CO_2 reduction by **2** with Mg^{2+} is $2CO_2 + Mg^{2+} + 2e^- \rightarrow CO + MgCO_3$, as evidenced by IR-SEC and CPE experiments (vide infra). It is likely that our electrochemical solutions have small amounts of H_2O, and therefore, the thermodynamic reaction described by Costentin et al. (without taking into account Mg^{2+}) is a very good approximation for our catalytic reaction. To the best of our knowledge, the standard reduction potential for $2CO_2 + 2e^- \rightarrow CO + CO_3^{2-}$ has not been determined in MeCN due to unavailable free energy thermodynamic values in MeCN. For an estimation of the overpotential for our catalytic reaction, substitution of the CO_3^{2-} product with HCO_3^- using the thermodynamic reaction described by Costentin et al. is adequate. In MeCN, the standard reduction potential for $2CO_2 + H_2O + 2e^- \rightarrow CO + H_2O + CO_3^{2-}$ is E° = −0.65 V versus NHE (or approximately −1.3 V vs $Fc^{+/0}$).[39] To account for the thermodynamics of $MgCO_3$ formation in the catalytic reaction (vide infra), we can calculate the difference in free energy of formation for $MgCO_3$ versus $Mg^{2+} + CO_3^{2-}$ in aqueous solution (approximately −29 kJ/mol).[40] This difference corresponds to a potential change of approximately 150 mV, and thus, E° = −1.15 V versus $Fc^{+/0}$. However, it is important to stress that this correction takes into account free energy values in aqueous solution, not in acetonitrile, and therefore, we will estimate E° for our catalytic reaction as −1.15 − −1.3 V versus $Fc^{+/0}$. By using this estimated standard potential, at −1.6 V versus $Fc^{+/0}$, **2** operates with an overpotential η = 0.3−0.45 V. At this overpotential, **2** displays one of the lowest overpotentials for CO_2 reduction to CO for a homogeneous electrocatalyst. Other electrocatalysts that exhibit relatively low overpotentials are $[Ni(cyclam)]^{2+}$,[41] $[Co^{III}(N_4H)(Br)_2]^+$,[42] and Re(bpy)$(CO)_3$Cl operating in neat 1-ethyl-3-methylimidazolium tetracyanoborate ionic liquid (each operating at approximately η = 0.5 V).[43] Table S1 lists the overpotentials of a variety of other commonly studied CO_2 reduction electrocatalysts. Catalyst **2** operates with a 0.05−0.2 V lower overpotential than the lowest operating homogeneous CO_2 reduction electrocatalyst previously reported.

Infrared Spectroelectrochemistry (IR-SEC) with Added Mg^{2+}. IR-SEC of complex **1** under N_2 with added Mg^{2+} was performed to observe how the reductive chemistry of **1** is altered by the presence of Mg^{2+} (Figure 6). At its resting state,

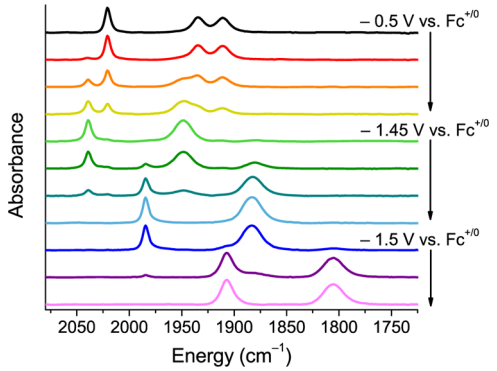

Figure 6. IR-SEC of 3 mM complex **1** in MeCN with 0.1 M $TBAPF_6$ electrolyte and 0.1 M $Mg(OTf)_2$ under an atmosphere of N_2. Solvolysis of the Mn−Br bond in resting species **1** (pink) occurs over time in solution to form $[Mn(mesbpy)(CO)_3(MeCN)]^+$ (teal). At −1.45 V, the Mn(I) complex is reduced to the radical species, $[Mn(mesbpy)(CO)_3]^0$ (yellow). At slightly more negative potentials (−1.5 V), this Mn radical species is reduced to the anionic complex, $[Mn(mesbpy)(CO)_3]^-$ (black).

1 has three characteristic ν_{CO} bands associated with a facially coordinated tricarbonyl complex at 2023, 1936, and 1913 cm^{-1}. Before reaching the potential of the two-electron reduction seen in CVs, solvolysis of the Mn−Br bond occurs, resulting in the formation of a cationic Mn−NCMe complex (ν_{CO} = 2039, 1949 cm^{-1}). When the potential of the cell reaches approximately −1.45 V versus $Fc^{+/0}$, we see growth of ν_{CO} bands at 1984 and 1883 cm^{-1}, along with decay of the ν_{CO} bands associated with the cationic Mn−MeCN complex. These new ν_{CO} bands are consistent with the formation of the singly reduced Mn(0) complex, $[Mn(mesbpy)(CO)_3]^0$. In previous IR-SEC experiments in the absence of Mg^{2+}, complete formation of this singly reduced Mn(0) complex was not observed.[28] Instead, only a small amount of singly reduced complex was observed along with concomitant formation of the doubly reduced complex, $[Mn(mesbpy)(CO)_3]^-$. In these IR-SEC studies, with added Mg^{2+}, we see complete and stable formation of $[Mn(mesbpy)(CO)_3]^0$ (Figure 6). Not until the potential of the cell is shifted slightly further negative (approximately −1.5 V vs $Fc^{+/0}$) is reduction of $[Mn(mesbpy)(CO)_3]^0$ to $[Mn(mesbpy)(CO)_3]^-$ observed (ν_{CO} = 1907, 1805 cm^{-1}). The fact that complete formation of $[Mn(mesbpy)(CO)_3]^0$ is observed prior to conversion to $[Mn(mesbpy)(CO)_3]^-$ indicates that Mg^{2+} is stabilizing the singly-reduced Mn(0) complex. This helps explain the prewave observed in CVs with added Mg^{2+} (Figures 4 and 5), where Mg^{2+} likely splits the two-electron reduction of **1** and **2** into two closely spaced one-electron reductions. The specific interaction between the singly-reduced Mn(0) complex and Mg^{2+} is currently under investigation.

DOI: 10.1021/jacs.5b12215
J. Am. Chem. Soc. 2016, 138, 1386−1393

We further utilized IR-SEC under CO_2 with added Mg^{2+} to gain insight into electrocatalysis in the presence of Mg^{2+}. The results of an IR-SEC experiment on complex **1** with added ~0.14 M CO_2 (half-saturated) and 0.1 M Mg^{2+} are shown in Figure 7. Initially, prior to reaching the reduction potential of

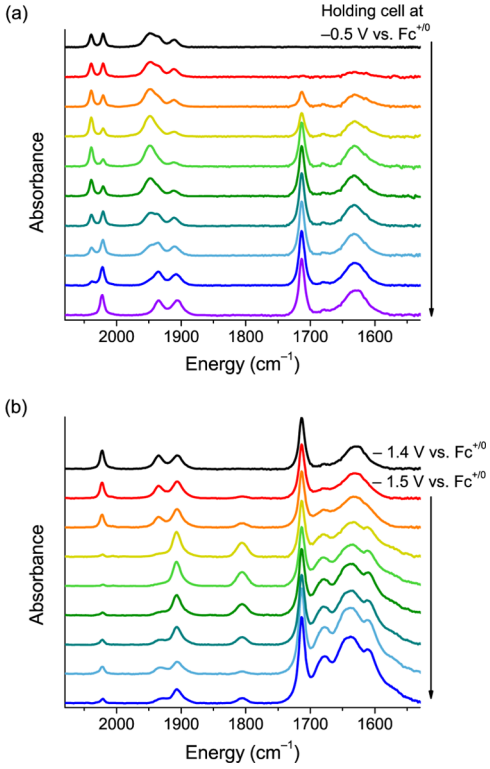

Figure 7. IR-SEC of 3 mM complex **1** in MeCN with 0.1 M $TBAPF_6$ electrolyte, 0.1 M $Mg(OTf)_2$, and about 0.14 M CO_2 (half-saturation). (a) At −0.5 V, a mixture of **1** and $[Mn(mesbpy)(CO)_3(MeCN)]^+$ exists. Holding the cell at this potential results in the formation of CO_3^{2-}/HCO_3^{2-} species. (b) By holding the cell at −1.5 V, catalytic formation of CO_3^{2-}/HCO_3^{2-} species is observed consistent with reductive disproportionation of $2CO_2$ to CO and CO_3^{2-}.

complex **1**, partial solvolysis of the Mn−Br bond is observed to form a cationic Mn−NCMe complex, similarly to what was observed in IR-SEC experiments under N_2 (Figure 6). Additionally, at these potentials, formation of IR bands at 1713 and 1632 cm^{-1} is observed. The IR band at 1632 cm^{-1} is consistent with HCO_3^-, formed from the reaction of Mg^{2+} with CO_2 in the presence of trace H_2O.[44] We tentatively assign the IR band at 1713 cm^{-1} to soluble $MgCO_3$, which reaches a maximum concentration due to poor solubility and remains unchanged during the course of the reaction. The exact identity of this band is still under investigation; however, oxalate and other reduced CO_2 species have been ruled out due to comparative IR experiments (Figure S10) and quantitative CO production observed in CPE experiments (vide infra). The species at 1713 and 1632 cm^{-1} are also observed upon stirring a solution of Mg^{2+} with CO_2 in 0.1 M $TBAPF_6$/MeCN overnight (Figure S10). These IR bands remain unchanged upon pulling vacuum on the reaction mixture, indicating that these products are the result of an irreversible reaction with Mg^{2+} and CO_2, which rules out the presence of a type of activated/coordinated CO_2 species.[45,46] The IR band at 1713 cm^{-1} remains unchanged upon addition of H_2O to the reaction mixture (Figure S17), consistent with the formation of a soluble $MgCO_3$-type species, which is present at a constant concentration due to an equilibrium with excess Mg^{2+} and CO_2 available in solution. Holding the IR-SEC cell at −0.5 V versus $Fc^{+/0}$ for over 5 min (and upon moving the potential of the cell to −1.4 V vs $Fc^{+/0}$) results in these species reaching equilibrium (Figure 7b).

Upon reaching the reduction potential of **1** at approximately −1.5 V versus $Fc^{+/0}$, we see complete conversion of the complex **1** to two new species that, on the basis of the ν_{CO} spectrum, must be a new Mn(I) complex and doubly-reduced $[Mn(mesbpy)(CO)_3]^-$ (Figure 7b). These two complexes are evidenced by the ν_{CO} bands at 2022, 1933, 1907, and 1805 cm^{-1}. This new Mn(I) complex is very similar to the Mn(I)−COOH complex formed in electrocatalysis with CO_2 and weak Brønsted acids (ν_{CO} = 2006, 1907 cm^{-1}). We have tentatively assigned this Mn(I) complex as $[Mn(I)-CO_2Mg]^+$ since C−O bond cleavage in the bound CO_2 ligand is likely the rate-determining step in the catalytic reaction.[28,29] Along with the formation of these two ν_{CO} bands, we see catalytic growth of IR bands at 1679, 1632, and 1611 cm^{-1}, which is consistent with the formation of CO_3^{2-} and HCO_3^- species. Catalytic formation of CO_3^{2-}-type species and a catalytic reaction that has a second order dependence on $[CO_2]$ are consistent with an overall reductive disproportionation of $2CO_2 + 2e^- \rightarrow CO + CO_3^{2-}$. Repeating IR-SEC experiments with $^{13}CO_2$ indicate that the CO_3^{2-} and HCO_3^- species originate from the starting $^{13}CO_2$ substrate (Figures S8 and S9).

Controlled Potential Electrolysis (CPE) with Added Mg^{2+}. CPE was performed on **2** at −1.6 V versus $Fc^{+/0}$ to confirm that the electrocatalytic reaction was indeed producing CO and to measure the efficiency at which CO is produced. First attempts at CPE resulted in very short-lived catalysis due to the formation of insoluble $MgCO_3$. To circumvent this issue, a sacrificial Mg rod, in conjunction with added $Mg(OTf)_2$, was used as the counter electrode in place of the Pt wire typically used (schematic in Figure S11). CPE experiments with this sacrificial Mg anode showed fairly stable current densities up to 6 h of electrolysis (Figure 8).

GC indicates that little hydrogen is formed during these experiments (Faradaic efficiency = 1%, TON for H_2 = 0.35). Catalyst **2** operates with a Faradaic efficiency of 98 ± 3% for

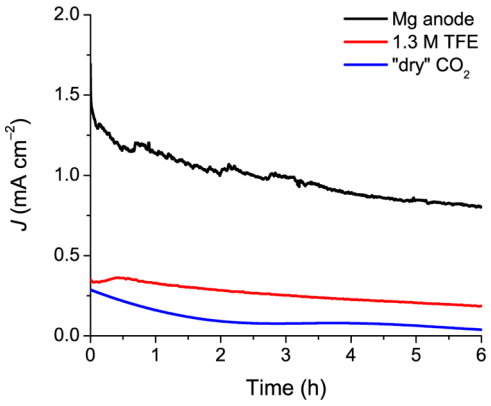

Figure 8. CPE current density over time for 0.5 mM $[Mn(mesbpy)(CO)_3(MeCN)](OTf)$ (**2**) under CO_2 with a sacrificial Mg anode and 0.2 M Mg^{2+} (black), added TFE (red), and without added TFE (blue). Conditions: potential = −1.6 V versus $Fc^{+/0}$; 0.1 M $TBAPF_6$/MeCN; working electrode = glassy carbon; counter electrode = Mg anode (black) or Pt (red and blue); reference electrode = Ag/AgCl.

DOI: 10.1021/jacs.5b12215
J. Am. Chem. Soc. 2016, 138, 1386−1393

the formation of CO from CO_2, measured through approximately 6 h of electrolysis (Figure S12). The catalyst sustained current densities greater than 1 mA/cm^2 throughout the first few hours of electrolysis (Figure 8). With the sacrificial Mg anode, TON for CO production reached ~36 after 6 h of electrolysis, significantly out-performing CPE experiments at −1.6 V versus $Fc^{+/0}$ with added TFE (TON = ~14 after 6 h, Figure S13). CPE experiments under N_2 with added $Mg(OTf)_2$ and the sacrificial Mg anode showed minimal CO formation over 6 h of electrolysis (Figure S13), indicating that degradation of the $Mn(CO)_3$ moiety does not occur in these experiments. Slow current decrease in CPE experiments under CO_2 with the sacrificial Mg anode is likely an effect of the sacrificial electrode rather than catalyst degradation (Figure S14). FTIR analysis of the postelectrolysis solution and particulates formed during CPE confirms the formation of CO_3^{2-} and HCO_3^- salts (Figure S14), displaying similar IR bands as those observed in IR-SEC experiments.

Catalytic Tafel Behavior. The low overpotential exhibited by catalyst **2** in the presence of Mg^{2+} led us to create catalytic Tafel plots to benchmark this catalyst with other commonly studied catalysts in terms of TOF and η. Costentin and Savéant have developed foot-of-the-wave analysis (FOWA)[2,39,47,48] to determination the Tafel behavior of catalysts that do not display idealized 'S-shaped' CVs (i.e., those that experience a variety of side phenomena that interfere with catalysis at high current densities). Because the catalytic CVs of **2** with added Mg^{2+} display nearly ideal 'S-shaped' catalytic waves, we can determine the Tafel behavior of our catalysis based on solely the plateau peak current values (described in more detail in the Supporting Information, Figures S15–S16. Our analysis leads to the Tafel plots shown in Figures 9, S15, and S16 at the two extremes of

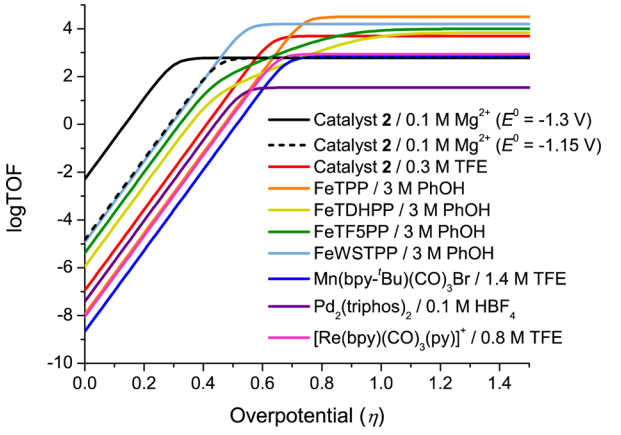

Figure 9. Catalytic Tafel plots for **2** with added Mg^{2+} and other commonly studied homogeneous CO_2 reduction electrocatalysts.[49] Volts are reported versus $Fc^{+/0}$. TPP = tetraphenylporphyrin, TDHPP = 5,10,15,20-tetrakis(2′,6′-dihydroxylphenyl)porphyrin, TF5PP = 5,15-bis(2′,6′-dihydroxyphenyl)-10,20-bis(pentrafluorophenyl)-porphyrin, WSTPP = 5,10,15,20-tetra(4′-*N*,*N*,*N*-trimethylanilinium)-porhyrin, bpy-*t*Bu = 4,4′-*tert*-butyl-2,2′-bipyridine, triphos = $C_6H_4\{P[CH_2CH_2P(C_6H_{11})_2]_2\}_2$.

the overpotential range estimated for this catalysis. The low overpotential for catalyst **2** with added Mg^{2+} is obvious when comparing its Tafel behavior with other catalysts' Tafel behaviors,[49] as shown in Figure 9. Under these conditions, catalyst **2** possesses a log TOF_0 = −2.3 − −4.8 (at E° = −1.3 V and −1.15 vs $Fc^{+/0}$, respectively) and log TOF_{max} = 2.8. The log TOF_0 and log TOF_{max} values of the other catalysts shown in Figure 9 are listed in Table S2.

CONCLUSIONS

We have described the use of a Lewis acid, $Mg(OTf)_2$, to significantly increase the catalytic rate for CO_2 reduction for $Mn(mesbpy)(CO)_3Br$ (**1**) and $[Mn(mesbpy)(CO)_3(MeCN)](OTf)$ (**2**) at low overpotentials. In previous studies, with weak Brønsted acids, catalysts **1** and **2** showed little to no reactivity for CO_2 reduction upon CO_2 binding at −1.6 V versus $Fc^{+/0}$. With the use of a glassy carbon working electrode with high surface area, we demonstrated using CPE that "slow catalysis" occurs upon CO_2 binding with added TFE. The rate of this catalysis is increased by over 10-fold by utilizing Mg^{2+} cations in place of TFE. At an operating potential of −1.6 V versus $Fc^{+/0}$, these Mn catalysts operate with the lowest overpotential (η = 0.3–0.45 V) for homogeneous electrocatalysts for CO_2 reduction. Variable concentration CV studies, IR-SEC experiments, and CPE have allowed us to conclude that electrocatalysis with added Mg^{2+} proceeds via a reductive disproportionation mechanism of $2CO_2 + 2e^- \rightarrow CO + CO_3^{2-}$, as shown in the mechanism in Figure 10. Here, CO_2

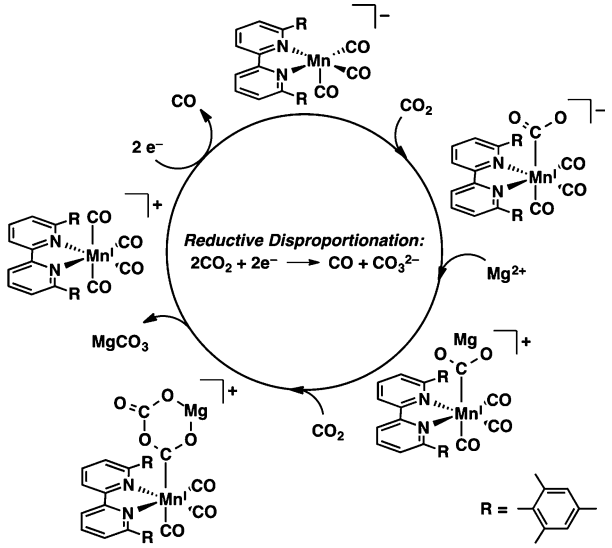

Figure 10. Proposed catalytic mechanism of $[Mn(mesbpy)(CO)_3]^-$ with CO_2 and Mg^{2+} at −1.5 V versus $Fc^{+/0}$, showing an overall catalytic reaction of $2CO_2 + 2e^- \rightarrow CO + CO_3^{2-}$.

binds to the active $[Mn(mesbpy)(CO)_3]^-$ catalyst and is capped by a Mg^{2+} cation. At this point, the Mg^{2+} cation has already aided in weakening a C–O bond of the bound CO_2 molecule. The addition of a second CO_2 molecule completes the breaking of a C–O bond, resulting in CO_3^{2-} formation in the form of $MgCO_3$. The resulting cationic Mn(I) tetracarbonyl complex is easily reduced at the operating potentials, releasing the CO product and regenerating the active catalyst.

The role played by Mg^{2+} cations in this catalytic reaction is a rare example of heterobimetallic chemical catalysis of an electrochemical reaction, where in an electron-rich center (Mn bpy framework) initiates the reduction process, and an electron-deficient center (Mg^{2+}) aids in bond transformation (cleavage of a C–O bond). In this reaction, Mg^{2+} plays the role of a cosubstrate rather than that of a cocatalyst. The findings in this work will allow for the exploration of Lewis acids to facilitate and enhance catalysis that requires the assistance of an

DOI: 10.1021/jacs.5b12215
J. Am. Chem. Soc. 2016, 138, 1386–1393

oxide acceptor (in our case, weak Brønsted acids). We believe this strategy can be applied to a wide variety of catalytic systems, not only for CO_2 reduction. These studies and findings provide strategies and mechanistic insights for improving catalysts for eventual scale-up and use on an industrial scale. Future work will focus on investigating softer Lewis acids, which will not bind carbonate salts as strongly as Mg^{2+} as well as applying this cosubtrate strategy to other CO_2 reduction systems.

EXPERIMENTAL SECTION

General Considerations. Solvents were sparged with argon, dried on a custom dry solvent system over alumina columns, and stored over molecular sieves before use. Synthesis of 6,6′-dimesityl-2,2′-bipyridine (mesbpy) was performed by the Suzuki coupling of 6,6′-dibromo-2,2′-bipyridine with trimethylphenylboronic acid, as previously reported.[37] Syntheses of Mn(mesbpy)$(CO)_3$Br (**1**) and [Mn(mesbpy)-$(CO)_3$(MeCN)](OTf) (**2**) were performed as previously reported.[28,37] Manipulations of Mn complexes were covered from light. Tetrabutylammonium hexafluorophosphate ($TBAPF_6$, Aldrich, 98%) was twice recrystallized from methanol (MeOH) and dried under a vacuum at 90 °C overnight before use. Magnesium triflate ($Mg(OTf)_2$, Aldrich, 97%) was dried in a vacuum oven at 100 °C overnight before use. All other chemicals were purchased from commercial sources and used as received. IR spectra were collected on a Thermo Scientific Nicolet 6700.

Electrochemistry. Electrochemical experiments were performed using a BASi Epsilon potentiostat. A single-compartment cell was used for all CV experiments with a glassy carbon working electrode (3 mm in diameter disc from BASi), a Pt wire counter electrode (flame annealed with a butane torch and separated from the bulk solution by a Vycor tip), and a Ag/AgCl leakless reference electrode (eDAQ, Inc.). Ferrocene (Fc) was added as an internal reference. All electrochemical experiments were performed with 0.1 M $TBAPF_6$ as the supporting electrolyte. Electrochemical cells were shielded from light during experiments. All solutions were purged with N_2 or "bone dry" CO_2 (each run through a custom Drierite/activated 3 Å molecular sieves drying column) before CVs were taken. All potentials were referenced versus $Fc^{+/0}$.

Bulk Electrolysis. Bulk electrolysis experiments (at ca. −1.6 V vs $Fc^{+/0}$) were carried out in a 60 mL Gamry five-neck cell equipped with three Ace-Thred ports to hold each electrode and two joints capable of being sealed with septa for gas sparging. This setup included a glassy carbon working electrode (surface area = ∼80 mm), either a Pt wire counter electrode (flame annealed with a butane torch before use and separated from the bulk solution by porous frit) or a sacrificial Mg rod, and a Ag/AgCl leakless reference electrode (eDAQ, Inc.). A BASi Epsilon potentiostat was used to apply potential and record current. These bulk electrolysis experiments were carried out in 30 mL of MeCN with 0.1 M $TBAPF_6$ with the appropriate amount of either TFE or $Mg(OTf)_2$. Bulk electrolysis solutions were purged with either dry N_2 or dry CO_2 for 10 min prior to electrolysis. Solutions were constantly stirred and shielded from light throughout bulk electrolysis experiments. Gas analysis for bulk electrolysis experiments were performed using 1 mL sample injections on a Hewlett-Packard 7890A Series gas chromatograph with two molsieve columns (30 m × 0.53 mm ID × 25 μm film). The 1 mL injection was split between two columns, one with N_2 as the carrier gas and one with He as the carrier gas, to quantify both H_2 and CO simultaneously in each run. GC calibration curves were made by sampling known volumes of CO and H_2 gas.

Infrared Spectroelectrochemistry (IR-SEC). The design of the IR spectroelectrochemical cell used for these studies has been reported previously by our group.[22] The working electrode for the cell was a 4.5 mm glassy carbon disk. All spectroelectrochemical experiments were carried out in a 0.1 M $TBAPF_6$ solution in MeCN with 0.1 M $Mg(OTf)_2$, and all solutions were prepared under an atmosphere of dry nitrogen in a glovebox. Blank MeCN solutions with 0.1 M $TBAPF_6$ and 0.1 M $Mg(OTf)_2$ were used for the FTIR solvent subtractions. For experiments under CO_2, a solution of catalyst in $TBAPF_6/Mg(OTf)_2$/MeCN was saturated with CO_2 (ca. 0.28 M) and diluted in half by an N_2-sparged solution of $TBAPF_6/Mg(OTf)_2$/MeCN, affording a solution of about 0.14 M CO_2. A Gamry Reference 600 series three electrode potentiostat was used to affect and monitor thin layer bulk electrolysis.

ASSOCIATED CONTENT

Supporting Information

The Supporting Information is available free of charge on the ACS Publications website at DOI: 10.1021/jacs.5b12215.

Experimental details on TOF calculations and catalytic Tafel plots and supporting figures and tables for CPE, CV, and IR-SEC experiments (PDF)

AUTHOR INFORMATION

Corresponding Author

*ckubiak@ucsd.edu

Notes

The authors declare no competing financial interest.

ACKNOWLEDGMENTS

This work was supported by the Air Force Office of Scientific Research through the MURI program under AFOSR Award No. FA9550-10-1-0572. The authors thank Dr. Charles W. Machan for the insight and helpful discussions.

REFERENCES

(1) Benson, E. E.; Kubiak, C. P.; Sathrum, A. J.; Smieja, J. M. *Chem. Soc. Rev.* **2009**, *38*, 89−99.
(2) Costentin, C.; Robert, M.; Saveant, J.-M. *Chem. Soc. Rev.* **2013**, *42*, 2423−2436.
(3) Rakowski Dubois, M.; Dubois, D. L. *Acc. Chem. Res.* **2009**, *42*, 1974−1982.
(4) Hod, I.; Sampson, M. D.; Deria, P.; Kubiak, C. P.; Farha, O. K.; Hupp, J. T. *ACS Catal.* **2015**, *5*, 6302−6309.
(5) Chen, Z.; Concepcion, J. J.; Jurss, J. W.; Meyer, T. J. *J. Am. Chem. Soc.* **2009**, *131*, 15580−15581.
(6) Lieber, C. M.; Lewis, N. S. *J. Am. Chem. Soc.* **1984**, *106*, 5033−5034.
(7) Yoshida, T.; Tsutsumida, K.; Teratani, S.; Yasufuku, K.; Kaneko, M. *J. Chem. Soc., Chem. Commun.* **1993**, 631−633.
(8) Lin, S.; Diercks, C. S.; Zhang, Y.-B.; Kornienko, N.; Nichols, E. M.; Zhao, Y.; Paris, A. R.; Kim, D.; Yang, P.; Yaghi, O. M.; Chang, C. J. *Science* **2015**, *349*, 1208−1213.
(9) Kornienko, N.; Zhao, Y.; Kley, C. S.; Zhu, C.; Kim, D.; Lin, S.; Chang, C. J.; Yaghi, O. M.; Yang, P. *J. Am. Chem. Soc.* **2015**, *137*, 14129−14135.
(10) Chabolla, S. A.; Dellamary, E. A.; Machan, C. W.; Tezcan, F. A.; Kubiak, C. P. *Inorg. Chim. Acta* **2014**, *422*, 109−113.
(11) Wong, K.-Y.; Chung, W.-H.; Lau, C.-P. *J. Electroanal. Chem.* **1998**, *453*, 161−169.
(12) Benson, E. E.; Grice, K. A.; Smieja, J. M.; Kubiak, C. P. *Polyhedron* **2013**, *58*, 229−234.
(13) Benson, E. E.; Kubiak, C. P. *Chem. Commun.* **2012**, *48*, 7374−7376.
(14) Hawecker, J.; Lehn, J. M.; Ziessel, R. *J. Chem. Soc., Chem. Commun.* **1984**, 328−330.
(15) Machan, C. W.; Chabolla, S. A.; Yin, J.; Gilson, M. K.; Tezcan, F. A.; Kubiak, C. P. *J. Am. Chem. Soc.* **2014**, *136*, 14598−14607.
(16) Sampson, M. D.; Froehlich, J. D.; Smieja, J. M.; Benson, E. E.; Sharp, I. D.; Kubiak, C. P. *Energy Environ. Sci.* **2013**, *6*, 3748−3755.
(17) Smieja, J. M.; Benson, E. E.; Kumar, B.; Grice, K. A.; Seu, C. S.; Miller, A. J. M.; Mayer, J. M.; Kubiak, C. P. *Proc. Natl. Acad. Sci. U. S. A.* **2012**, *109*, 15646−15650.

DOI: 10.1021/jacs.5b12215
J. Am. Chem. Soc. 2016, 138, 1386−1393

(18) Smieja, J. M.; Kubiak, C. P. *Inorg. Chem.* **2010**, *49*, 9283−9289.
(19) Sullivan, B. P.; Bolinger, C. M.; Conrad, D.; Vining, W. J.; Meyer, T. J. *J. Chem. Soc., Chem. Commun.* **1985**, 1414−1416.
(20) Benson, E. E.; Sampson, M. D.; Grice, K. A.; Smieja, J. M.; Froehlich, J. D.; Friebel, D.; Keith, J. A.; Carter, E. A.; Nilsson, A.; Kubiak, C. P. *Angew. Chem., Int. Ed.* **2013**, *52*, 4841−4844.
(21) Johnson, F. P. A.; George, M. W.; Hartl, F.; Turner, J. J. *Organometallics* **1996**, *15*, 3374−3387.
(22) Machan, C. W.; Sampson, M. D.; Chabolla, S. A.; Dang, T.; Kubiak, C. P. *Organometallics* **2014**, *33*, 4550−4559.
(23) Keith, J. A.; Grice, K. A.; Kubiak, C. P.; Carter, E. A. *J. Am. Chem. Soc.* **2013**, *135*, 15823−15829.
(24) Bourrez, M.; Molton, F.; Chardon-Noblat, S.; Deronzier, A. *Angew. Chem., Int. Ed.* **2011**, *50*, 9903−9906.
(25) Bourrez, M.; Orio, M.; Molton, F.; Vezin, H.; Duboc, C.; Deronzier, A.; Chardon-Noblat, S. *Angew. Chem., Int. Ed.* **2014**, *53*, 240−243.
(26) Grice, K. A.; Kubiak, C. P. *Adv. Inorg. Chem.* **2014**, *66*, 163−188.
(27) Smieja, J. M.; Sampson, M. D.; Grice, K. A.; Benson, E. E.; Froehlich, J. D.; Kubiak, C. P. *Inorg. Chem.* **2013**, *52*, 2484−2491.
(28) Sampson, M. D.; Nguyen, A. D.; Grice, K. A.; Moore, C. E.; Rheingold, A. L.; Kubiak, C. P. *J. Am. Chem. Soc.* **2014**, *136*, 5460−5471.
(29) Riplinger, C.; Sampson, M. D.; Ritzmann, A. M.; Kubiak, C. P.; Carter, E. A. *J. Am. Chem. Soc.* **2014**, *136*, 16285−16298.
(30) Takeda, H.; Koizumi, H.; Okamoto, K.; Ishitani, O. *Chem. Commun.* **2014**, *50*, 1491−1493.
(31) Fei, H.; Sampson, M. D.; Lee, Y.; Kubiak, C. P.; Cohen, S. M. *Inorg. Chem.* **2015**, *54*, 6821−6828.
(32) Hartl, F.; Rosa, P.; Ricard, L.; Le Floch, P.; Záliš, S. *Coord. Chem. Rev.* **2007**, *251*, 557−576.
(33) Machan, C. W.; Sampson, M. D.; Kubiak, C. P. *J. Am. Chem. Soc.* **2015**, *137*, 8564−8571.
(34) Kuramochi, Y.; Itabashi, J.; Fukaya, K.; Enomoto, A.; Yoshida, M.; Ishida, H. *Chem. Sci.* **2015**, *6*, 3063−3074.
(35) Sampson, M. D.; Kubiak, C. P. *Inorg. Chem.* **2015**, *54*, 6674−6676.
(36) Hammouche, M.; Lexa, D.; Momenteau, M.; Saveant, J. M. *J. Am. Chem. Soc.* **1991**, *113*, 8455−8466.
(37) Schmittel, M.; Ganz, A.; Schenk, W. A.; Hagel, M. *Z. Naturforsch., B: J. Chem. Sci.* **1999**, *54*, 559−564.
(38) Espension, J. H. *Chemical Kinetics and Reaction Mechanisms*; McGraw−Hill: New York, 1981.
(39) Costentin, C.; Drouet, S.; Robert, M.; Savéant, J.-M. *Science* **2012**, *338*, 90−94.
(40) *CRC Handbook of Chemistry and Physics*; 92nd ed.; Haynes, W. M., Ed.; CRC Press: Boca Raton, FL, 2011−2012.
(41) Froehlich, J. D.; Kubiak, C. P. *Inorg. Chem.* **2012**, *51*, 3932−3934.
(42) Lacy, D. C.; McCrory, C. C. L.; Peters, J. C. *Inorg. Chem.* **2014**, *53*, 4980−4988.
(43) Grills, D. C.; Matsubara, Y.; Kuwahara, Y.; Golisz, S. R.; Kurtz, D. A.; Mello, B. A. *J. Phys. Chem. Lett.* **2014**, *5*, 2033−2038.
(44) Ferrini, V.; De Vito, C.; Mignardi, S. *J. Hazard. Mater.* **2009**, *168*, 832−837.
(45) Dossmann Soldi-Lose, H.; Afonso, C.; Lesage, D.; Tabet, J.-C.; Uggerud, E. *Angew. Chem., Int. Ed.* **2012**, *51*, 6938−6941.
(46) Miller, G. B. S.; Esser, T. K.; Knorke, H.; Gewinner, S.; Schöllkopf, W.; Heine, N.; Asmis, K. R.; Uggerud, E. *Angew. Chem., Int. Ed.* **2014**, *53*, 14407−14410.
(47) Costentin, C.; Drouet, S.; Robert, M.; Savéant, J.-M. *J. Am. Chem. Soc.* **2012**, *134*, 11235−11242.
(48) Costentin, C.; Savéant, J.-M. *ChemElectroChem* **2014**, *1*, 1226−1236.
(49) Costentin, C.; Robert, M.; Savéant, J.-M.; Tatin, A. *Proc. Natl. Acad. Sci. U. S. A.* **2015**, *112*, 6882−6886.

DOI: 10.1021/jacs.5b12215
J. Am. Chem. Soc. 2016, 138, 1386−1393